Journal of Applied Physics

RESEARCH ARTICLE | JANUARY 23 2025

Strain tuning of oxygen vacancy channels in $SrCoO_{2.5}$ thin films

Rajan Mishra ; Shivam Choudhary ; Sourav Chowdhury ; Anju Ahlawat ; Anupam Jana ; Angelo Giglia ; Stefano Nannarone; Moritz Hoesch ; Ram Janay Choudhary

J. Appl. Phys. 137, 045301 (2025)
https://doi.org/10.1063/5.0249995

AIP Publishing

Journal of Applied Physics ARTICLE pubs.aip.org/aip/jap

Strain tuning of oxygen vacancy channels in $SrCoO_{2.5}$ thin films

Cite as: J. Appl. Phys. **137**, 045301 (2025); doi: 10.1063/5.0249995
Submitted: 21 November 2024 · Accepted: 5 January 2025 ·
Published Online: 23 January 2025

Rajan Mishra,[1] Shivam Choudhary,[1] Sourav Chowdhury,[2,a)] Anju Ahlawat,[3] Anupam Jana,[4] Angelo Giglia,[4] Stefano Nannarone,[4] Moritz Hoesch,[2] and Ram Janay Choudhary[1,a)]

AFFILIATIONS

[1]UGC-DAE Consortium for Scientific Research, University Campus, Khandwa Road, Indore, Madhya Pradesh 452001, India
[2]Deutsches Elektronen-Synchrotron DESY, Notkestraβe 85, Hamburg 22607, Germany
[3]Department of Physics, Sage University, Kailod Kartal, Indore-Dewas By-Pass Road, Indore, Madhya Pradesh 452020, India
[4]CNR—Istituto Officina dei Materiali (IOM), S.S. 14 km–163.5, Basovizza, Trieste 34149, Italy

[a)]**Authors to whom correspondence should be addressed:** sourav.chowdhury@desy.de and ram@csr.res.in

ABSTRACT

Tuning of the oxygen vacancy channels (OVCs) ordering is crucial to control ionic conduction, which has much promise in energy materials and memory devices. Brownmillerite (BM) oxides have been proven to be an ideal playground for exploring the modulation of OVCs through external stimuli. In the BM-$SrCoO_{2.5}$ thin films, we observed that in-plane compressive strain promotes horizontal OVCs, while in-plane tensile strain facilitates vertical OVCs. The modulation of the OVCs can also be made through electric biasing utilizing the piezostrain. The selective regulation of the orientation of the OVCs in BM-$SrCoO_{2.5}$ thin films through strain engineering will significantly enhance the development and implementation of functional features for ion transport and migration-related functionality.

I. INTRODUCTION

Oxygen vacancies in transition-metal oxides (TMOs) significantly affect electronic device performance. For instance, solid-oxide fuel cells, memristors, field-effect transistors, and gas sensors are governed by the chemical potential of oxygen vacancy formation and their transport.[1–4] Oxygen vacancies are also thought to be involved in fatigue and other processes for high dielectrics and ferroelectric constants.[5,6] Understanding the atomistic oxygen transport mechanisms in TMOs requires knowledge of the distributions of oxygen vacancies in the system. Oxygen vacancies are not just defects in materials; they play a significant role in influencing the mechanical, optical, electrical, and catalytic properties of materials.[3,7] High degrees of oxygen vacancy ordering and alternate cation sequences lead to the formation of oxygen vacancy channels (OVCs) that offer quick pathways for oxygen transport, enhancing the kinetics of processes such as surface exchange and oxygen ion diffusion.[8]

In this context, brownmillerite (BM) oxides are particularly interesting for their ability to host a high density of well-organized OVCs at typical perovskite (P) lattice sites through the topotactic phase transition.[9–13] The topotactic phase transition in $SrCoO_x$ between the insulating-antiferromagnet BM-$SrCoO_{2.5}$ ($SCO_{2.5}$) and the metallic-ferromagnet P-$SrCoO_3$ (SCO_3) end members promotes these materials in a wide range of applications, such as solid-oxide fuel cells, neuromorphic computation, Mottronics, memory devices, and smart window materials.[9–16]

Tuning the physical and chemical properties of orthorhombic BM oxides is significantly influenced by the regulation of their OVCs. The BM structure features alternating octahedral (O_h) and tetrahedral (T_d) layers, with the T_d layers containing fully ordered oxygen vacancies that create one-dimensional OVCs.[13–18] The BM structure has variable lattice constants with respect to the crystal axis; hence, it is noteworthy that a different crystal plane of the substrate is used to obtain a distinct orientation of the OVCs of the BM films on the substrate. Furthermore, direct evidence of the function of oxygen vacancies and surface structure in the surface oxygen exchange process may be obtained by the selective exposure of oxygen vacancies through orientation control.[7] In addition to its entwined structural, electronic, and magnetic properties, BM-$SCO_{2.5}$ demonstrates a fascinating tunable electrical and magnetic phase via

strain in thin film form.[18–21] Various factors, such as surface energy, the crystallographic orientation of the substrate, and epitaxial strain, can influence the OVC ordering.[22]

The OVCs in the BM structure are tilted 45° with respect to the chain of the T_d units, and by changing its orientation, a greater ionic conductivity may be obtained along the OVCs.[8] When the orientation of the OVCs is regulated to maximize the catalytic activity and ionic transport, this anisotropic crystal structure can offer an open-structured surface that is catalytically beneficial. The OVCs created in these structures facilitate rapid ionic diffusion and ion storage, offering potential applications in fuel cells, rechargeable batteries, oxygen separation membranes, and solid-oxide fuel cells.[23,24] The OVCs have also a significant impact on magnetic anisotropy and the resistive switching response in memristors.[25,26] Furthermore, solid solutions based on spin-crossover materials can also be utilized in solid-oxide fuel cells and solid-oxide electrolysis cells due to their high oxygen mobility and favorable structural and electronic characteristics.[27] Thus, a deeper comprehension of the oxygen-diffusion mechanism at the microscopic level would significantly enhance the development and implementation of functional features for energy conversion and anion insertion applications.

In earlier studies in $SrCoO_x$ systems, researchers employed liquid ion gating (ILG) to switch the OVCs from horizontal to vertical.[28] In this study, we divulge that the OVCs can be changed via strain tuning by growing the thin films on various single crystal substrates, producing different strain conditions on the BM-$SCO_{2.5}$ thin films. It is observed that BM-$SCO_{2.5}$ thin films grown on substrates such as $(LaAlO_3)_{0.3}(Sr_2TaAlO_6)_{0.7}$ (LSAT) and $SrTiO_3$ (STO), which produce in-plane compressive strain, result in horizontal OVCs in the system, referred to as H-$SCO_{2.5}$.[19,20,29,30] However, for the SCO thin film deposited on substrates like $[Pb(Mg_{1/3}Nb_{2/3})O_3]_{0.70}$–$[PbTiO_3]_{0.30}$ (PMN-PT) and $BaTiO_3$ (BTO), which induce in-plane tensile strain, the OVCs transformed to a vertical orientation, termed V-$SCO_{2.5}$. The V-$SCO_{2.5}$ phase is confirmed through crystallographic, magnetic, and electronic characterizations. Our study offers a clean engineering approach for modulating OVCs in BM oxides.

II. EXPERIMENTAL

We deposited the thin films of BM-$SCO_{2.5}$ of thickness range of 20–25 nm on (001) oriented LSAT, STO, PMN-PT, and BTO substrates using the pulsed laser deposition (PLD) method equipped with a KrF excimer laser, ($\lambda \sim 248$ nm, 20 ns pulse width) (Coherence, USA). We choose such a thickness range to produce strained thin films. The BM-$SCO_{2.5}$ target prepared via solid-state reaction route was used for the thin film deposition. The deposition parameters were as follows: substrate temperature of 750 °C, base pressure of 2×10^{-7} Torr in the chamber before deposition, an oxygen partial pressure of 150 mTorr during the deposition, a laser fluence of 2 J/cm^2, and a target to substrate distance of 5 cm. The grown films were cooled at the same 150 mTorr of O_2 partial pressure. For comparison, we have also prepared a thin film of P-SCO_3 on the STO substrate from the corresponding BM-$SCO_{2.5}$ film following the route mentioned in Ref. 13. The crystalline phase was identified by a Bruker D2 Phaser x-ray diffractometer equipped with Cu K_α ($\lambda = 1.5406$ Å) radiation. The in-plane phi scans and the oblique pane θ–2θ x-ray diffraction (XRD) were carried out by using a Bruker D8-Discover high-resolution x-ray diffractometer equipped with Cu K_α radiation. The ambient condition x-ray absorption spectroscopy (XAS) studies across the Co $L_{3,2}$ and O K edges were carried out at 300 K in the surface sensitive (probing depth ~5 nm) total electron yield (TEY) mode by measuring the sample drain current at the beamline BL-01, Indus-2 at RRCAT, Indore, India. The energy resolution during the XAS measurements across the Co $L_{3,2}$-edges and O K-edge was estimated to be ~300 and ~250 meV, respectively. The electric bias-dependent XAS measurements were performed at the BEAR beamline, Elettra, Trieste, Italy, in the TEY mode at the Co $L_{3,2}$-edges and O K-edge at 300 K. The spectra were taken at grazing incidence by fixing the angle between the sample surface and the incident beam to 45°. The photon energies were calibrated using the known energy peak positions of the Co $L_{3,2}$-edges and the O K-edge of Co_3O_4, which are 779.5 and 529.9 eV, respectively. We employed magnetic measurements utilizing a 7 T SQUID-VSM system from Quantum Design, Inc. in the USA. The applied magnetic field was parallel to the film's surface.

III. RESULTS AND DISCUSSION

Figure 1(a) shows the θ–2θ XRD patterns of the BM-$SCO_{2.5}$ thin films deposited on (001) oriented LSAT, STO, PMN-PT, and BTO substrates along with P-SCO_3 thin film deposited on the STO (001) substrate. For the films deposited on LSAT and STO, we observed twofold superstructure peaks such as (002), (006), and (0010) in addition to (004) and (008) peaks, which are caused by the oxygen defects ordering. Such a unique XRD pattern is the fingerprint of the presence of the BM phase with alternate repetition of O_h and T_d units along the crystallographic c-axis, namely, H-$SCO_{2.5}$.[9,10,30] Interestingly, the films deposited on BTO and PMN-PT substrates do not exhibit such twofold superstructure peaks. However, the three Bragg reflections obtained in the XRD patterns of the thin films on BTO and PMN-PT substrates do match with the V-$SCO_{2.5}$ phase.[28] It should be noted here that such an XRD pattern is also very similar to the P-SCO_3 phase among the members of the $SrCoO_x$ series. However, these thin films were prepared simultaneously in the same deposition condition, and getting oxygen-reach P-SCO_3 phase formation requires a two-step process: the preparation of the BM-$SCO_{2.5}$ phase followed by further oxidizing it in an ambient O_2-atmosphere after deposition in the PLD chamber.[9,31] Thus, obtaining the P-SCO_3 phase in the one-step deposition process is highly unlikely. We have further confirmed the V-$SCO_{2.5}$ phase of the films on BTO and PMN-PT substrates later in the manuscript. The calculated c lattice parameters of BM-$SCO_{2.5}$ thin films on LSAT, STO, BTO, and PMN-PT substrates are 3.963, 3.935, 3.805, and 3.797 Å, respectively. In addition, the out-of-plane strain on LSAT, STO, BTO, and PMN-PT substrates is calculated as 0.96, 0, −3.05, and −3.35%, respectively.

The BM-$SCO_{2.5}$ thin films, which are subjected to in-plane compressive strain on LSAT and STO substrates, or even relaxed BM-$SCO_{2.5}$ thin film, show the H-$SCO_{2.5}$ phase.[9,30–32] The detailed structural studies of the thin films on LSAT and STO substrates can be found elsewhere.[20,29] However, there is no report in the literature on the BM-$SCO_{2.5}$ film grown on a substrate that produces

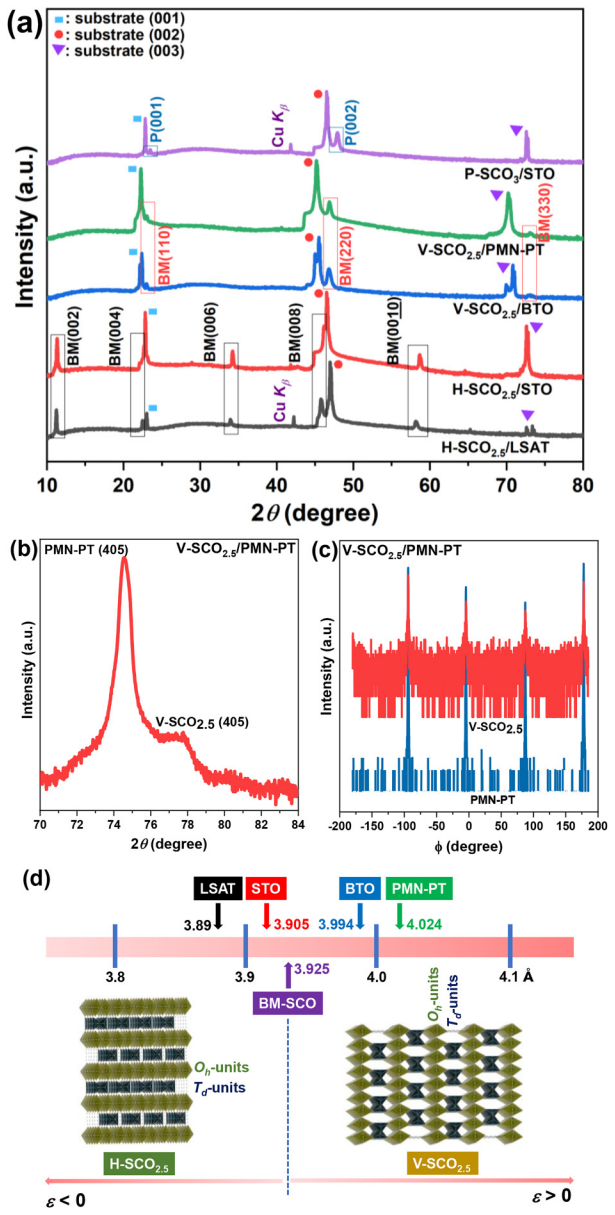

FIG. 1. (a) X-ray diffraction (XRD) patterns of BM-$SrCoO_{2.5}$ and P-$SrCoO_3$ thin films on different substrates such as $(LaAlO_3)_{0.3}(Sr_2TaAlO_6)_{0.7}$ (LSAT), $SrTiO_3$ (STO), $Pb(Mg_{1/3}Nb_{2/3})O_3$-$PbTiO_3$ (PMN-PT), and $BaTiO_3$ (BTO) of (001) orientations. The brownmillerite and perovskite peaks are denoted as BM and P, respectively. Here, H-$SCO_{2.5}$ and V-$SCO_{2.5}$ stand for BM-$SrCoO_{2.5}$ with horizontal and vertical oxygen vacancy channels (OVCs), respectively. (b) The oblique plane (405), θ–2θ XRD patterns of the V-$SCO_{2.5}$/PMN-PT thin film. (c) In-plane phi scan of the V-$SCO_{2.5}$/PMN-PT thin film and PMN-PT substrate. The film's reflections coincide with the substrate's reflections indicating the cube-on-cube growth of the V-$SCO_{2.5}$ film on the PMN-PT substrate. (d) Schematic representation of strain tuning of OVCs in BM-$SCO_{2.5}$ between the H-$SCO_{2.5}$ and V-$SCO_{2.5}$ phases. The in-plane compressive ($\varepsilon < 0$) and tensile strain ($\varepsilon > 0$) stabilize H-$SCO_{2.5}$ and V-$SCO_{2.5}$ phases, respectively. Lattice parameters of the BM-$SCO_{2.5}$ bulk and the single crystal substrates are mentioned.

in-plane tensile strain. BTO and PMN-PT have in-plane lattice parameters of 3.994 and 4.024 Å, respectively, which is larger than the same of BM-$SCO_{2.5}$, which is 3.925 Å in the pseudo-tetragonal notation.[30] Thus, the BM-$SCO_{2.5}$ films on such substrates should experience in-plane tensile strain, which we confirmed from the oblique angle θ–2θ XRD pattern of the BM-$SCO_{2.5}$/PMN-PT system across the (405) reflections of both the film and substrate as shown in Fig. 1(b). The calculated in-plane strain (ε) in the BM-$SCO_{2.5}$ film on the PMN-PT substrate is ~2.42%. Furthermore, we also performed an in-plane phi scan as shown in Fig. 1(c); the film's reflections coincide with the substrate's reflections indicating cube-on-cube growth of the V-$SCO_{2.5}$ film on the PMN-PT substrate. Figure 1(d) shows the schematic view of the H-$SCO_{2.5}$ to V-$SCO_{2.5}$ phase transformation due to strain. In-plane compressive strain stabilizes the horizontal OVCs, H-$SCO_{2.5}$, whereas in-plane tensile strain stabilizes the vertical OVCs, V-$SCO_{2.5}$.

The magnetization (M) vs temperature (T) measurements are crucial in determining the phases of grown thin films. We recorded the M–T measurements at field (H) = 1000 Oe of H-$SCO_{2.5}$, V-$SCO_{2.5}$, and P-SCO_3 as shown in Fig. 2(a). The P-SCO_3 film shows usual ferromagnetic behavior with Curie temperature, $T_C \sim 250$ K; and the H-$SCO_{2.5}$ and V-$SCO_{2.5}$ show almost negligible moment as compared to the P-SCO_3 phase due to the expected antiferromagnetic nature of the H-$SCO_{2.5}$ and V-$SCO_{2.5}$ phases with the Neel temperature of $T_N \sim 570$ K.[9,18,32] We also recorded the M–H hysteresis behavior at $T = 5$ K of the thin films as shown in Fig. 2(b). Consistent with M–T data, M–H also revealed the ferromagnetic nature of the P-SCO_3 thin film and the antiferromagnetic nature of H-$SCO_{2.5}$ and V-$SCO_{2.5}$ thin films. Thus, the magnetic measurements further confirm that the film grown on PMN-PT is, indeed, V-$SCO_{2.5}$ and not P-SCO_3.

Figure 2(c) displays the Co $L_{3,2}$-edges XAS of the H-$SCO_{2.5}$, V-$SCO_{2.5}$, and P-SCO_3 thin films. The Co $L_{3,2}$-edge XAS yields the spin–orbit split components L_2 (Co-$2p_{1/2} \rightarrow$ Co-3d) and L_3 (Co-$2p_{3/2} \rightarrow$ Co-3d), which correspond to the transition of electrons from the Co-2p core level to the unoccupied states of Co-3d. The features and the peak positions of H-$SCO_{2.5}$ and V-$SCO_{2.5}$ are quite similar and are distinct from the P-SCO_3 film. Moreover, the L_3-edge peak position is about 1 eV higher in the P-SCO_3 film than in the H-$SCO_{2.5}$ and V-$SCO_{2.5}$ films. In addition, the 2p spin–orbit splitting, the separation between L_3 and L_2 features, is lower in P-SCO_3 relative to H-$SCO_{2.5}$ and V-$SCO_{2.5}$ films. These observations confirmed a change state difference of ~1 unit of Co between P-SCO_3 and H-$SCO_{2.5}$ (and/or V-$SCO_{2.5}$) thin films.[9,23] We also examined the O K-edge XAS of the H-$SCO_{2.5}$, V-$SCO_{2.5}$, and P-SCO_3 thin films as shown in Fig. 2(d). The O K-edge XAS yields the transition of an electron from the O-1s core level to the unoccupied O-2p states hybridized with different bands of Co and Sr, as indicated in Fig. 2(d).[33–35] The first broad feature at position 530.4 eV is the O-2p-Co-3d hybridized band. The second feature at 534.9 eV is the O-2p-Sr 4d hybridized band, and a broad feature (537–546 eV) is attributed to the O-2p-Co 4sp and O-2p-Co 4s hybridized states.[33,34]

So far, we have seen that the switching between H-$SCO_{2.5}$ and V-$SCO_{2.5}$ phases can be done through the substrate induced epitaxial strain tuning. PMN-PT is a ferroelectric material, so its lattice

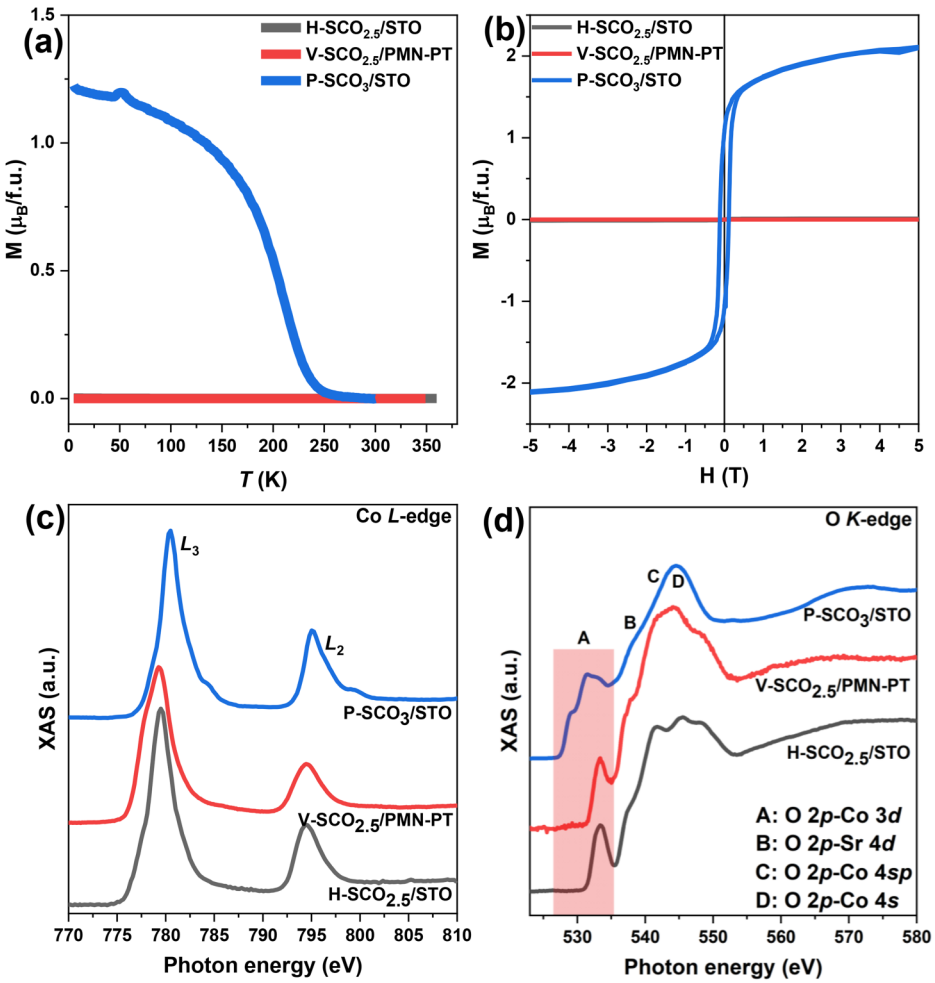

FIG. 2. (a) Magnetization (M) vs temperature (T) curves of H-$SCO_{2.5}$/STO, V-$SCO_{2.5}$/PMN-PT, and P-SCO_3/STO thin films in the field cooled warming (FCW) cycle measured at magnetic field H = 1000 Oe. (b) M–H hysteresis curves of the thin films at 5 K. Room temperature total electron yield (TEY) x-ray absorption spectra (XAS) of the thin films at (c) Co $L_{3,2}$-edges and (d) O *K*-edge.

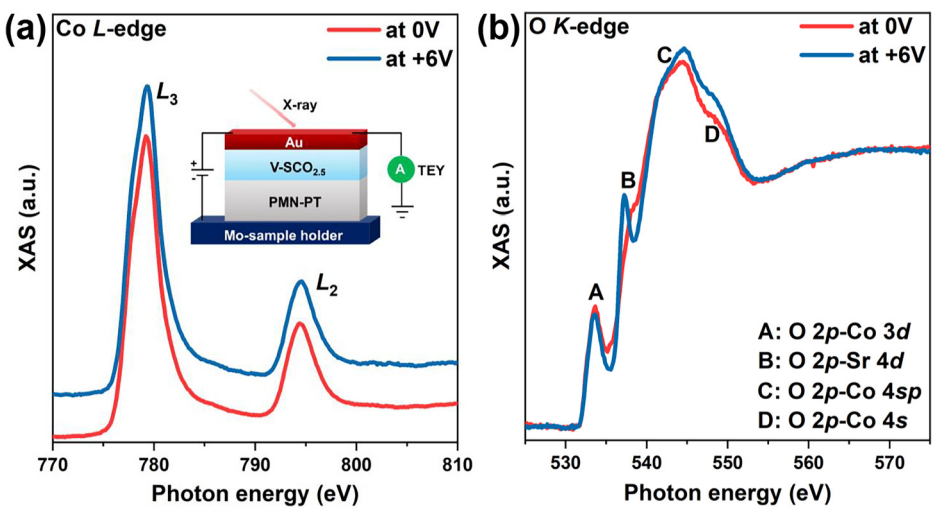

FIG. 3. Electric bias-dependent room temperature TEY XAS of V-$SCO_{2.5}$/PMN-PT thin film at (a) Co $L_{3,2}$-edges and (b) O *K*-edge. The schematic of the sample configuration is shown in the inset in (a).

parameter can be changed with an electric field.[36] The change in the lattice parameter of the PMN-PT substrate might also shift the strain state on the V-$SCO_{2.5}$ thin film with electric biasing. Thus, the inverse piezoelectric strain could switch the OVCs in the BM-$SCO_{2.5}$ systems by tuning the electric bias. To look into this aspect, we performed electric bias-dependent XAS in an Au/V-$SCO_{2.5}$/PMN-PT system across the Co $L_{3,2}$-edges and O K-edge at room temperature as shown in Figs. 3(a) and 3(b). The schematic of the sample configuration for the bias-dependent XAS measurements is shown in the inset in Fig. 3(a) where Au serves as the top electrode and Mo-sample holder as the bottom electrode. It can be seen in Fig. 3(a) that the Co $L_{3,2}$-edges remain almost unaffected with bias application of 6 V across the sample. However, the O K-edge shows considerable changes in Fig. 3(b). This is attributed to the local structural rearrangements in the V-$SCO_{2.5}$ thin film upon electric biasing, which is caused by the PMN-PT substrate's inverse piezoelectric effect induced strain in the V-$SCO_{2.5}$ thin film. The induced strain affects the hybridization between the O, Co, and Sr orbitals. Our study showcases the possible pathway to switch the OVCs in BM-$SCO_{2.5}$ systems through ferroelectric strain tuning. This observed local strain effect is different from the interface change rearrangement effect due to electric biasing observed in the other oxide thin film systems on ferroelectric substrates.[37,38]

The orientation of the polyhedral of O_h and T_d units in the BM structure depends strongly on the crystal symmetry and strain state.[22,28,39] Regulating the lattice strain can change the orientation of the OVCs in the BM thin films by reducing the system's free energy. The H-$SCO_{2.5}$ and V-$SCO_{2.5}$ phase stabilization in in-plane compressive and tensile strained conditions, respectively, could be due to the modulation in the energy barrier, allowing V-$SCO_{2.5}$ O_2 to migrate directly from the substrate into the OVCs without needing to traverse the O_h layers.

IV. CONCLUSIONS

In summary, it is demonstrated that the rearrangement of the OVCs can be made through substrate induced strain engineering in the BM-$SrCoO_{2.5}$ thin films. Horizontal OVCs, H-$SCO_{2.5}$, are stabilized by in-plane compressive strain, whereas vertical OVCs, V-$SCO_{2.5}$, are stabilized by in-plane tensile strain. The modulation of the OVCs can also be made through electric biasing utilizing the piezoelectric substrate. The selective rearrangements of the OVCs in BM-$SrCoO_{2.5}$ thin films will make this system a promising candidate for future energy technology and memory applications.

ACKNOWLEDGMENTS

The authors thank A. Wadikar and R. Sah for helping with XAS measurements. The authors acknowledge DST-SERB for the grant under Project No. CRG/2021/001021. R.M. and R.J.C. acknowledge the Indo-Italian Program of Cooperation grant from the Italian Ministry of Foreign Affairs and International Cooperation and the Indian Department of Science & Technology for performing the beamtime at BEAR beamline, Elettra synchrotron, Trieste, Italy, under Proposal ID: 20235266.

AUTHOR DECLARATIONS

Conflict of Interest

The authors have no conflicts to disclose.

Author Contributions

Rajan Mishra: Conceptualization (lead); Data curation (lead); Formal analysis (lead); Investigation (lead); Methodology (lead); Resources (lead); Software (lead); Validation (lead); Visualization (lead); Writing – original draft (lead); Writing – review & editing (lead). **Shivam Choudhary:** Data curation (equal); Formal analysis (equal); Investigation (supporting); Methodology (supporting); Software (supporting); Validation (supporting); Visualization (supporting); Writing – review & editing (supporting). **Sourav Chowdhury:** Conceptualization (equal); Data curation (equal); Formal analysis (equal); Investigation (equal); Methodology (equal); Resources (equal); Software (equal); Supervision (equal); Validation (equal); Visualization (equal); Writing – original draft (equal); Writing – review & editing (equal). **Anju Ahlawat:** Formal analysis (supporting); Investigation (supporting); Methodology (supporting); Resources (supporting); Software (supporting); Validation (supporting); Visualization (supporting); Writing – review & editing (supporting). **Anupam Jana:** Data curation (supporting); Investigation (supporting); Resources (supporting); Validation (supporting); Writing – review & editing (supporting). **Angelo Giglia:** Data curation (supporting); Software (supporting); Validation (supporting); Writing – review & editing (supporting). **Stefano Nannarone:** Data curation (supporting); Validation (supporting); Writing – review & editing (supporting). **Moritz Hoesch:** Validation (supporting); Writing – review & editing (supporting). **Ram Janay Choudhary:** Conceptualization (equal); Data curation (equal); Formal analysis (equal); Funding acquisition (equal); Investigation (equal); Methodology (equal); Project administration (equal); Resources (equal); Software (equal); Supervision (equal); Validation (equal); Visualization (equal); Writing – original draft (equal); Writing – review & editing (equal).

DATA AVAILABILITY

The data that support the findings of this study are available from the corresponding authors upon reasonable request.

REFERENCES

[1]J. E. Auckett, A. J. Studer, E. Pellegrini, J. Ollivier, M. R. Johnson, H. Schober, W. Miiller, and C. D. Ling, "Combined experimental and computational study of oxide ion conduction dynamics in $Sr_2Fe_2O_5$ brownmillerite," Chem. Mater. **25**, 3080 (2013).

[2]N. R. Venkata, T. Octolia, L. Chunli, P. B. Ho, P. Ji-Yong, C. Yunae, K. Dong-Wook, J. Janghyun, K. Deok-Hwang, and K. Miyoung, "Epitaxial brownmillerite oxide thin films for reliable switching memory," ACS Appl. Mater. Interfaces **8**, 7902 (2016).

[3]J. Walter, S. Bose, M. Cabero, G. Yu, M. Greven, M. Varela, and C. Leighton, "Perpendicular magnetic anisotropy via strain-engineered oxygen vacancy ordering in epitaxial $La_{1-x}Sr_xCoO_{3-\delta}$," Phys. Rev. Mater. **2**, 111404 (2018).

[4]X. Wu, J. Walter, T. Feng, J. Zhu, H. Zheng, J. F. Mitchell, N. Biškup, M. Varela, X. Ruan, C. Leighton, and X. Wang, "Glass-like through-plane thermal conductivity induced by oxygen vacancies in nanoscale epitaxial $La_{0.5}Sr_{0.5}CoO_{3-\delta}$," Adv. Funct. Mater. **27**, 1704233 (2017).

[5]N. C. Bristowe, P. B. Littlewood, and E. Artacho, "Surface defects and conduction in polar oxide heterostructures," Phys. Rev. B **83**, 205405 (2011).
[6]S. Fabiano, N. Sani, J. Kawahara, L. Kergoat, J. Nissa, I. Engquist, X. Crispin, and M. Berggren, "Ferroelectric polarization induces electronic nonlinearity in ion-doped conducting polymers," Sci. Adv. **3**, e1700345 (2017).
[7]J. Jeong, N. Aetukuri, T. Graf, T. D. Schladt, M. G. Samant, and S. S. Parkin, "Suppression of metal-insulator transition in VO_2 by electric field-induced oxygen vacancy formation," Science **339**, 1402 (2013).
[8]C. A. J. Fisher and M. S. Islam, "Mixed ionic/electronic conductors $Sr_2Fe_2O_5$ and $Sr_4Fe_6O_{13}$: Atomic-scale studies of defects and ion migration," J. Mater. Chem. **15**, 3200 (2005).
[9]H. Jeen, W. S. Choi, M. D. Biegalski, C. M. Folkman, I.-C. Tung, D. D. Fong, J. W. Freeland, D. Shin, H. Ohta, M. F. Chisholm, and H. N. Lee, "Reversible redox reactions in an epitaxially stabilized SrCoOx oxygen sponge," Nat. Mater. **12**, 1057 (2013).
[10]N. Lu, P. Zhang, Q. Zhang, R. Qiao, Q. He, H.-B. Li, Y. Wang, J. Guo, D. Zhang, Z. Duan, Z. Li, M. Wang, S. Yang, M. Yan, E. Arenholz, S. Zhou, W. Yang, L. Gu, C.-W. Nan, J. Wu, Y. Tokura, and P. Yu, "Electric-field control of tri-state phase transformation with a selective dual-ion switch," Nature **546**, 124 (2017).
[11]J. Suntivich, H. A. Gasteiger, N. Yabuuchi, H. Nakanishi, J. B. Goodenough, and Y. Shao-Horn, "Design principles for oxygen-reduction activity on perovskite oxide catalysts for fuel cells and metal–air batteries," Nat. Chem. **3**, 546 (2011).
[12]H. Y. Huang, C. Ge, Q. H. Zhang, C. X. Liu, J. Y. Du, J. K. Li, C. Wang, L. Gu, G. Z. Yang, and K. J. Jin, "Electrolyte-gated synaptic transistor with oxygen ions," Adv. Funct. Mater. **29**, 1902702 (2019).
[13]S. Chowdhury, A. Jana, A. Kumar Mandal, R. J. Choudhary, and D. M. Phase, "Electronic phase switching in the negative charge transfer energy $SrCoO_x$ thin films with the mottronic relevancies," ACS Appl. Electron. Mater. **3**, 3060 (2021).
[14]C. Ge, C. x. Liu, Q. l. Zhou, Q. h. Zhang, J. y. Du, J. k. Li, C. Wang, L. Gu, G. z. Yang, and K. j. Jin, "A ferrite synaptic transistor with topotactic transformation," Adv. Mater. **31**, 1900379 (2019).
[15]P. Scheiderer, M. Schmitt, J. Gabel, M. Zapf, M. Stübinger, P. Schütz, L. Dudy, C. Schlueter, T. L. Lee, and M. Sing, "Tailoring materials for mottronics: Excess oxygen doping of a prototypical Mott insulator," Adv. Mater. **30**(25), 1706708 (2018).
[16]J. Chen, W. Mao, L. Gao, F. Yan, T. Yajima, N. Chen, Z. Chen, H. Dong, B. Ge, P. Zhang, X. Cao, M. Wilde, Y. Jiang, T. Terai, and J. Shi, "Electron-doping mottronics in strongly correlated perovskite," Adv. Mater. **32**, 1905060 (2020).
[17]M. Hibino, R. Harimoto, Y. Ogasawara, R. Kido, A. Sugahara, T. Kudo, E. Tochigi, N. Shibata, Y. Ikuhara, and N. Mizuno, "A new rechargeable sodium battery utilizing reversible topotactic oxygen extraction/insertion of $CaFeO_z$ ($2.5 \le z \le 3$) in an organic electrolyte," J. Am. Chem. Soc. **136**, 488 (2014).
[18]S. Chowdhury, A. Jana, M. Kuila, V. R. Reddy, R. J. Choudhary, and D. M. Phase, "Negative charge-transfer energy in $SrCoO_{2.5}$ thin films: An interplay between O-2*p* hole density, charge-transfer energy, charge disproportionation, and ferromagnetic ordering," ACS Appl. Electron. Mater. **2**(12), 3859–3870 (2020).
[19]S. Chowdhury, R. J. Choudhary, and D. M. Phase, "Strain dependent spin-blockade effect realization in the charge-disproportionated $SrCoO_{2.5}$ thin films," Appl. Phys. Lett. **119**(2), 021901 (2021).
[20]S. Chowdhury, A. Jana, R. Rawat, P. Yadav, R. Islam, F. Xue, A. K. Mandal, S. Sarkar, R. Mishra, R. Venkatesh, D. M. Phase, and R. J. Choudhary, "High-temperature insulating ferromagnetic state in charge-disproportionated and spin-state-disproportionated strained $SrCoO_{2.5}$ thin film," APL Mater. **12**(5), 051129 (2024).
[21]S. Chowdhury, R. J. Choudhary, and D. M. Phase, "Spectroscopic aspects of the magnetic interaction in $SrCoO_{2.75}$ and $SrCoO_3$ thin films," J. Alloys Compd. **869**, 159296 (2021).
[22]J. Gazquez, S. Bose, M. Sharma, M. Torija, S. J. Pennycook, C. Leighton, and M. Varela, "Lattice mismatch accommodation via oxygen vacancy ordering in epitaxial $La_{0.5}Sr_{0.5}CoO_{3-\delta}$ thin films," APL Mater. **1**(1), 012105 (2013).
[23]S. Hu, W. Han, S. Hu, J. Seidel, J. Wang, R. Wu, J. Wang, J. Zhao, Z. Xu, M. Ye, and L. Chen, "Voltage-controlled oxygen non-stoichiometry in $SrCoO_{3-\delta}$ thin films," Chem. Mater. **31**(16), 6117–6123 (2019).
[24]B. Ma, N. I. Victory, U. Balachandran, B. J. Mitchell, and J. W. Richardson Jr., "Study of the mixed-conducting $SrFeCo_{0.5}O_y$ system," J. Am. Ceram. Soc. **85**(11), 2641–2645 (2002).
[25]S. K. Acharya, R. V. Nallagatla, O. Togibasa, B. W. Lee, C. Liu, C. U. Jung, B. H. Park, J.-Y. Park, Y. Cho, D.-W. Kim, J. Jo, D.-H. Kwon, M. Kim, C. S. Hwang, and S. C. Chae, "Epitaxial brownmillerite oxide thin films for reliable switching memory," ACS Appl. Mater. Interfaces **8**(12), 7902–7911 (2016).
[26]S. K. Acharya, J. Jo, N. V. Raveendra, U. Dash, M. Kim, H. Baik, S. Lee, B. H. Park, J. S. Lee, S. C. Chae, C. S. Hwang, and C. U. Jung, "Brownmillerite thin films as fast ion conductors for ultimate-performance resistance switching memory," Nanoscale **9**(29), 10502–10510 (2017).
[27]K. T. Lee and E. D. Wachsman, "Role of nanostructures on SOFC performance at reduced temperatures," MRS Bull. **39**(9), 783–791 (2014).
[28]H. Han, A. Sharma, H. L. Meyerheim, J. Yoon, H. Deniz, K.-R. Jeon, A. K. Sharma, K. Mohseni, C. Guillemard, M. Valvidares, P. Gargiani, and S. S. P. Parkin, "Control of oxygen vacancy ordering in brownmillerite thin films via ionic liquid gating," ACS Nano **16**(4), 6206–6214 (2022).
[29]S. Chowdhury, A. Jana, A. Kumar Mandal, S. Sarkar, R. J. Choudhary, and D. M. Phase, "Electronic, orbital, and spin reconstructions at the interface between metallic $La_{0.7}Sr_{0.3}MnO_3$ and charge-disproportionated insulator $SrCoO_{2.5}$," J. Phys. Chem. C **125**(31), 17537–17545 (2021).
[30]S. Chowdhury, S. Majumder, R. Mishra, A. K. Mandal, A. Bagri, S. Yadav, S. Karmarkar, D. Phase, and R. Choudhary, "Room temperature reversible colossal volto-magnetic effect in all-oxide metallicmagnet/topotactic-phase-transition material heterostructures," arXiv:2308.04324 (2023).
[31]Y. Wang, Q. He, W. Ming, M.-H. Du, N. Lu, C. Cafolla, J. Fujioka, Q. Zhang, D. Zhang, S. Shen, Y. Lyu, A. T. N'Diaye, E. Arenholz, L. Gu, C. Nan, Y. Tokura, S. Okamoto, and P. Yu, "Robust ferromagnetism in highly strained $SrCoO_3$ thin films," Phys. Rev. X **10**(2), 021030 (2020).
[32]S. Chowdhury, R. J. Choudhary, and D. M. Phase, "Time evolution of the structural, electronic, and magnetic phases in relaxed $SrCoO_3$ thin films," ACS Appl. Electron. Mater. **3**(11), 5095–5101 (2021).
[33]M. Abbate, G. Zampieri, J. Okamoto, A. Fujimori, S. Kawasaki, and M. Takano, "X-ray absorption of the negative charge-transfer material $SrFe_{1-x}Co_xO_3$," Phys. Rev. B **65**(16), 165120 (2002).
[34]S. Hu, Z. Yue, J. S. Lim, S. J. Callori, J. Bertinshaw, A. Ikeda-Ohno, T. Ohkochi, C.-H. Yang, X. Wang, C. Ulrich, and J. Seidel, "Growth and properties of fully strained $SrCoO_x$ ($x \approx 2.8$) thin films on $DyScO_3$," Adv. Mater. Interfaces **2**, 1500012 (2015).
[35]C. Mitra, T. Meyer, H. N. Lee, and F. A. Reboredo, "Oxygen diffusion pathways in brownmillerite $SrCoO_{2.5}$: Influence of structure and chemical potential," J. Chem. Phys. **141**, 084710 (2014).
[36]A. A. Levin, A. I. Pommrich, T. Weißbach, D. C. Meyer, and O. Bilani-Zeneli, "Reversible tuning of lattice strain in epitaxial $SrTiO_3/La_{0.7}Sr_{0.3}MnO_3$ thin films by converse piezoelectric effect of $0.72Pb(Mg_{1/3}Nb_{2/3})O_3-0.28PbTiO_3$ substrate," J. Appl. Phys. **103**(5), 054102 (2008).
[37]Z.-X. Xu, J.-M. Yan, M. Xu, L. Guo, T.-W. Chen, G.-Y. Gao, S.-N. Dong, M. Zheng, J.-X. Zhang, Y. Wang, X.-G. Li, H.-S. Luo, and R.-K. Zheng, "Integration of oxide semiconductor thin films with relaxor-based ferroelectric single crystals with large reversible and nonvolatile modulation of electronic properties," ACS Appl. Mater. Interfaces **10**, 32809 (2018).
[38]H. Ni, M. Zheng, L. Chen, W. Huang, Y. Qi, J. Zeng, Z. Tang, H. Lu, and J. Gao, "Large nonvolatile multiple-state resistive switching in $TiO_{2-\delta}$/PMN-PT field-effect device," Appl. Phys. Lett. **110**, 213503 (2017).
[39]L. Wang, Z. Yang, M. E. Bowden, and Y. Du, "Brownmillerite phase formation and evolution in epitaxial strontium ferrite heterostructures," Appl. Phys. Lett. **114**, 231602 (2019).